Bioorganic & Medicinal Chemistry 19 (2011) 6340–6347

Contents lists available at SciVerse ScienceDirect

Bioorganic & Medicinal Chemistry

journal homepage: www.elsevier.com/locate/bmc

Bioassay-guided identification of an anti-inflammatory prenylated acylphloroglucinol from *Melicope ptelefolia* and molecular insights into its interaction with 5-lipoxygenase

Khozirah Shaari [a,*], Velan Suppaiah [b], Lam Kok Wai [a,e], Johnson Stanslas [b], Bimo Ario Tejo [c], Daud Ahmad Israf [d], Faridah Abas [a], Intan Safinar Ismail [a], Nor Hasifi Shuaib [a], Seema Zareen [a], Nordin Hj. Lajis [a]

[a] Laboratory of Natural Products, Institute of Bioscience, Universiti Putra Malaysia, 43400 UPM Serdang, Selangor Darul Ehsan, Malaysia
[b] Pharmacotherapeutics Unit, Department of Medicine, Faculty of Medicine and Health Sciences, Universiti Putra Malaysia, 43400 UPM Serdang, Selangor Darul Ehsan, Malaysia
[c] Chemistry Department, Faculty of Science, Universiti Putra Malaysia, 43400 UPM Serdang, Selangor Darul Ehsan, Malaysia
[d] Department of Biomedical Science, Faculty of Medicine and Health Sciences, Universiti Putra Malaysia, 43400 UPM Serdang, Selangor Darul Ehsan, Malaysia
[e] Drug and Herbal Research Centre, Faculty of Pharmacy, Universiti Kebangsaan Malaysia, Jalan Raja Muda Abdul Aziz, 50300 Kuala Lumpur, Malaysia

ARTICLE INFO

Article history:
Received 4 July 2011
Revised 1 September 2011
Accepted 2 September 2011
Available online 10 September 2011

Keywords:
Melicope ptelefolia
Rutacecae
Acylpholoroglucinol
Anti-inflammatory
Lipoxygenase
Cyclooxygenase
Dual LOX/COX inhibitors

ABSTRACT

A bioassay-guided investigation of *Melicope ptelefolia* Champ ex Benth (Rutaceae) resulted in the identification of an acyphloroglucinol, 2,4,6-trihydroxy-3-geranylacetophenone or tHGA, as the active principle inhibiting soybean 15-LOX. The anti-inflammatory action was also demonstrated on human leukocytes, where the compound showed prominent inhibitory activity against human PBML 5-LOX, with an IC_{50} value of 0.42 μM, very close to the effect produced by the commonly used standard, NDGA. The compound concentration-dependently inhibited 5-LOX product synthesis, specifically inhibiting cysteinyl leukotriene LTC_4 with an IC_{50} value of 1.80 μM, and showed no cell toxicity effects. The anti-inflammatory action does not seem to proceed via redox or metal chelating mechanism since the compound tested negative for these bioactivities. Further tests on cyclooxygenases indicated that the compound acts via a dual LOX/COX inhibitory mechanism, with greater selectivity for 5-LOX and COX-2 (IC_{50} value of 0.40 μM). The molecular features that govern the 5-LOX inhibitory activity was thus explored using in silico docking experiments. The residues Ile 553 and Hie 252 were the most important residues in the interaction, each contributing significant energy values of −13.45 (electrostatic) and −5.40 kcal/mol (electrostatic and Van der Waals), respectively. The hydroxyl group of the phloroglucinol core of the compound forms a 2.56 Å hydrogen bond with the side chain of the carboxylate group of Ile 553. Both Ile 553 and Hie 252 are crucial amino acid residues which chelate with the metal ion in the active site. Distorting the geometry of these ligands could be the reason for the inhibition activity shown by tHGA. The molecular simulation studies supported the bioassay results and served as a good model for understanding the way tHGA binds in the active site of human 5-LOX enzyme.

1. Introduction

Melicope ptelefolia Champ ex Benth is a medium sized tree, common in Malaysia. The plant is used medicinally for treating menstrual disorders, remittent fevers, colds, rheumatism, itches and wounds.[1] Previously, we reported the presence of phenolic acids,[2] prenylated acylphloroglucinols,[3] furoquinoline alkaloids and flavonoids[4] from the plant. The plant also exhibited antioxidant,[4] antimicrobial[5] and antinociceptive[6] properties.

Lipoxygenase (LOX) is a group of closely related non-heme, iron containing dioxygenases catalyzing arachidonic acid metabolism. The enzyme inserts molecular oxygen at the fifth carbon, forming 5-hydroxyeicosatetraenoic acid (5-HETE). It then catalyzes a dehydration reaction, forming the unstable epoxide intermediate, leukotriene (LT) A_4[7] which is then further metabolized to the cysteinyl leukotrienes (CysLTs) by LTC_4 synthase.[8] Over the last decade, LOX inhibitors and leukotriene (LT) antagonists have become targets for rational drug design and discovery of mechanism-based drugs for treating chronic inflammatory diseases such as allergic asthma, psoriasis and rheumatoid arthritis.[9] The CysLTs in particular, comprising LTC_4, LTD_4 and LTE_4, are capable of inducing hyper-responsiveness, mucus secretion, edema, and eosinophilia, symptoms which are all seen in asthma.[10]

In our ongoing search for plants with potential use against asthma, the MeOH leaf extract of *M. ptelefolia* was screened for

* Corresponding author. Tel.: +603 8947 1248; fax: +603 8942 3552.
E-mail address: khozirah@science.upm.edu.my (K. Shaari).

0968-0896/$ - see front matter © 2011 Elsevier Ltd. All rights reserved.
doi:10.1016/j.bmc.2011.09.001

inhibition of soybean 15-lipoxygenase (15-LOX) activity. We describe herein the results of our investigation which included the bioassay-guided isolation of the anti-inflammatory constituent, its LOX inhibitory properties, its effect on 5-LOX product LTC_4 formation and its molecular interaction with the human enzyme 5-LOX.

2. Results and discussion

Several medicinal plant extracts were screened for anti-inflammatory activity using soybean 15-LOX assay (unpublished results). The leaf methanolic extract of *M. ptelefolia* was among several extracts that showed significant bioactivity. Thus, in pursuit of its bioactive constituent, the extract was subjected to further bioassay-guided fractionation and purification via standard chromatographic methods.

2.1. Bioassay-guided isolation of the LOX inhibitor from *M. ptelefolia*

At a test concentration of 100 μg/ml, the extract exhibited 72.3% inhibition of soybean 15-LOX activity (Table 1). Bioassay-guided fractionation, monitored by the same assay, indicated that the active components were localized in the CH_2Cl_2 fraction. The bioactivity of the CH_2Cl_2 fraction was observed to be dose-dependent.

Further chromatographic separation of the bioactive dichloromethane fraction yielded 2,4,6-trihydroxy-3-geranylacetophenone or tHGA (**1**), *p-O*-geranylcoumaric acid (**2**) (major constituent), kokusaginine (**3**) and scoparone (**4**) (Fig. 1). The compounds were all subsequently evaluated for soybean 15-LOX inhibitory activity. Only **1** was active against soybean 15-LOX, exhibiting a dose-dependent inhibitory activity with an IC_{50} value of 20.39 μM (Fig. 2), a value which is very close to the effect produced by the commonly used standard, NDGA (IC_{50} = 9.82 μM).

2.2. In vitro biological activity evaluations

2.2.1. Inhibitory effect on human PBML 5-LOX

Since the 15-LOX assay was carried out on a non-mammalian source of enzyme, this raised concern that the bioactivity may not be reproducible in a mammalian system. The compound tHGA (**1**) was thus tested further for inhibition of human PBML 5-LOX. Results showed that the compound inhibited the human enzyme with an IC_{50} value of 0.42 μM. In comparison to the standard drug NDGA (IC_{50} 0.12 μM), tHGA is therefore three and a half times less active (Fig. 3).

Table 1
In vitro 15-LOX inhibitory profile of the crude extract and fractions of *Melicope ptelefolia* in terms of % inhibition

Sample	Test concn (μg/ml)	% inhibition[a]
Crude MeOH	100	72.3 ± 0.7
Hexane	100	9.15 ± 1.0
	50	6.42 ± 0.7
	25	0.17 ± 7.8
CH_2Cl_2	100	57.02 ± 1.3
	50	55.03 ± 1.6
	25	39.26 ± 1.4
EtOAc	100	31.27 ± 1.0
	50	18.60 ± 5.1
	25	3.66 ± 4.1
Aqueous	100	18.42 ± 0.7
	50	10.79 ± 0.1
	25	4.47 ± 0.7
NDGA	25	88.84 ± 0.2

[a] Values are means ± SD of three independent experiments.

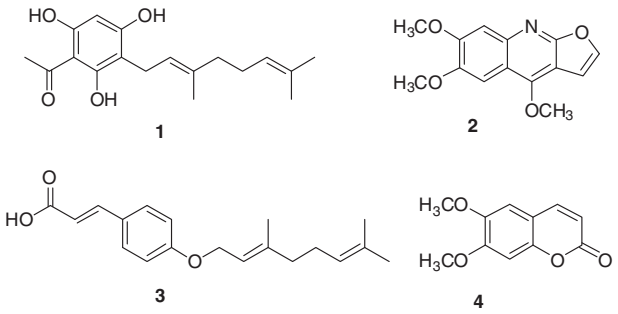

Figure 1. Compounds isolated from the bioactive CH_2Cl_2 fraction of *Melicope ptelefolia*.

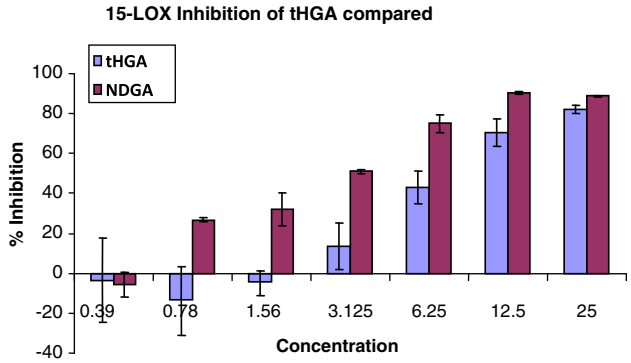

Figure 2. Inhibition of soybean 15-LOX by tHGA (**1**) compared to NDGA.

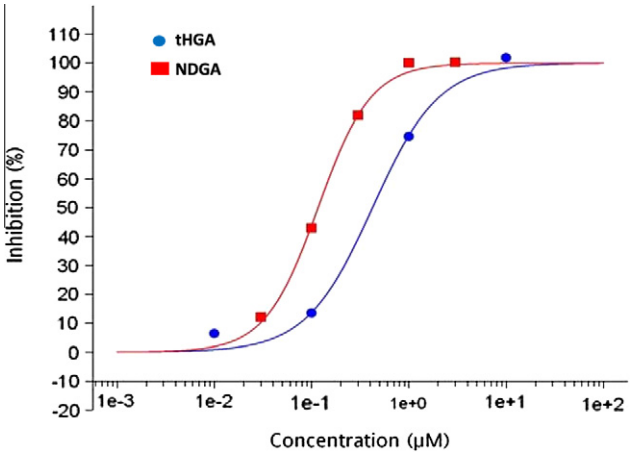

Figure 3. Inhibition of human PBML 5-LOX by tHGA (**1**) compared to NDGA. $n = 2$ (Supplementary data Fig. S4).

2.2.2. Inhibitory effect on formation of cysLTs

Investigation of the LOX inhibitory activity of the compound was extended further into its effect towards the formation of 5-LOX products of arachidonate metabolism. tHGA (**1**) showed significant dose-dependent reduction of LTC_4 production in calcium-stimulated mouse macrophages, without affecting macrophage viability (Fig. 4a). However, in comparison to the positive control, NDGA (IC_{50} 0.40 μM), tHGA (**1**) was four and a half times less active than in its effect, with an IC_{50} value of 1.80 μM.

2.2.3. Redox and metal-chelating abilities

Since inhibition of 5-LOX may proceed via redox or metal -chelating mechanisms, apart from competitive (non-redox) enzyme inhibition,[11] tHGA was also evaluated for its antioxidant

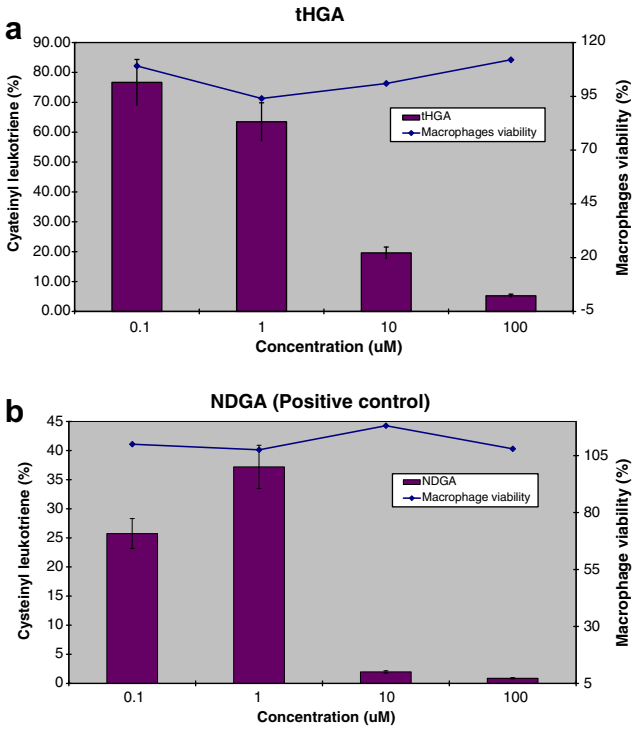

Figure 4. Effects of (a) tHGA (**1**) and (b) NDGA on LTC_4 release from calcium ionophore stimulated mouse macrophages. Inhibition percentages are expressed as mean values ± S.D. of three experiments.

and metal-chelating properties. The radical scavenging activity of tHGA (**1**) on stable DPPH free radical showed only moderate activity with an IC_{50} value of 46 μM in comparison to the positive control, quercetin which gave IC_{50} value of 6.91 μM. Meanwhile, addition of metal ions (Fe^{2+}, Fe^{3+} and Cu^{2+}) at a test concentration of 100 μm did not give rise to any changes in the absorbances or the intensity of UV-bands. This indicated that there is no complexation between tHGA (**1**) with the metal ions. Thus, a mechanism involving tHGA-Fe interaction for the enzyme inhibition was deduced to be unlikely.

2.2.4. Effect on prostaglandin biosynthesis

In addition to the LOX pathway, arachidonic acid metabolism can also proceed via the cyclooxygenase (COX) pathway. Cyclooxygenases catalyzes the conversion of arachidonic acid to form the cyclic endoperoxides, and subsequent metabolite products including prostaglandins and thromboxanes.[12] COX-1 is constitutively expressed in cells whereas COX-2 are inducible by certain cytokines, endotoxins, serum and growth factors. COX-2 inhibitors are more favorable as analgesic and anti-inflammatory agents since they have lesser side effects in comparison to COX-1 inhibitors.[13] Thus, the effects of tHGA (**1**) on the cyclooxygenases COX-1 and COX-2 were also examined (Figs. 5 and 6). Results revealed that tHGA (**1**) was as effective on COX-2, exhibiting an IC_{50} value of 0.40 μM while showing much lower activity against COX-1 (IC_{50} 6.9 μM). It appears that, although tHGA (**1**) acts as a dual LOX/COX inhibitor, it has better selectivity towards 5-LOX and COX-2.

2.3. Molecular modeling of the binding of tHGA on 5-LOX

For an insight into the 5-LOX inhibitory activity, the ligand-receptor interaction of the compound was investigated via molecular docking simulation studies.

The overall structure of human 5-LOX model was equilibrated after 2.0 ns (Fig. 7), with a root-mean square deviation (RMSD) of

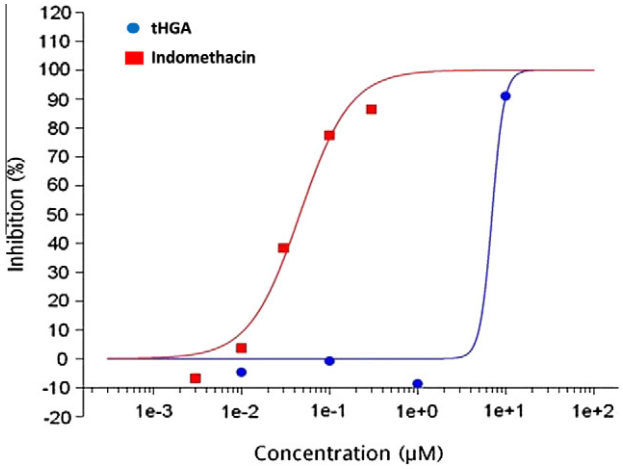

Figure 5. Inhibition of human PBML COX-1 by tHGA (**1**) compared to indomethacin. $n = 2$ (Supplementary data Fig. S4).

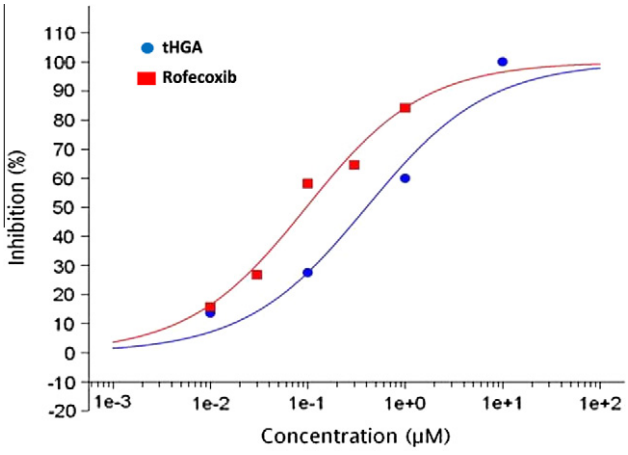

Figure 6. Inhibition of human PBML COX-2 by tHGA (**1**) compared to Rofecoxib. $n = 2$ (Supplementary data Fig. S4).

1.60 Å for the backbone atoms compared to the initial (Supplementary data, Fig. S1). The Ramachandran plot showed that the 5-LOX model is of high quality with 98.2% of the residues located inside the 'core' region (Supplementary data, Fig. S2). According to the mutagenesis studies and crystal structure analysis, the catalytic site of lipoxygenase comprised of two important con-

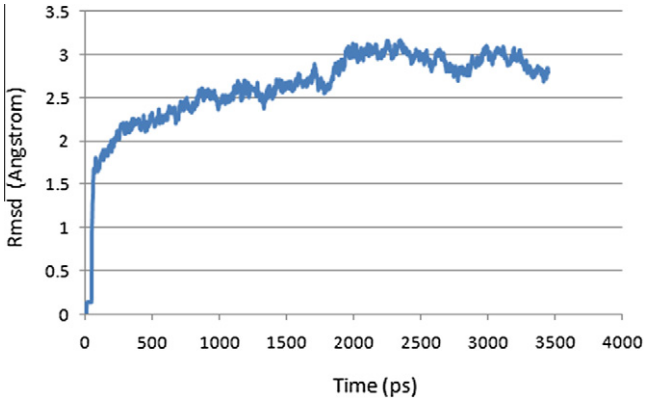

Figure 7. Total RMSD evolution along the simulation time.

served regions which included the Fe-binding site and the substrate binding cleft.[14] The structural geometry of the iron-binding site is highly conserved for any LOX enzyme where it has four amino acid ligands including the imidazole N-atoms of three histidine residues Hie247, Hie252 and Hie430 and the carboxylate oxygen of the C-terminal Ile553 which chelate with Fe. The substrate binding cleft was then defined as a 10 Å sphere comprising amino acid residues from the central position of the Fe-binding channel (Supplementary data, Table 1).

The binding interaction of tHGA (**1**), in the active pocket of the protein was investigated using GOLD program followed by energy minimization. The accuracy of the docking results depends strongly on the degree of the homology protein model. Based on the earlier negative results on metal-chelating activity shown by tHGA, we suggest that the enzyme inhibition shown by tHGA was most probably due to its capability of blocking the entry of the substrate in the active site with less effect on the chelation activity.

The MM-GBSA calculation is further employed to evaluate the free energy decomposition at the atomic level, especially the Van der Waals and electrostatic energy contribution in order to understand the interactions between the ligand and the residues in the binding site (Tables 1 and 2). The most important residue in the interaction is Ile553 with electrostatic interaction contributing a significant energy value of −13.45 kcal/mol. Further visual inspection using LIGPLOT (Fig. 8) shows that the hydroxyl group from the phloroglucinol moiety forms a 2.56 Å hydrogen bond with the side chain of the carboxylate group of Ile553. Another important residue is Hie252 with a −5.40 kcal/mol reduction in $\Delta G_{subtotal,\ GB}$ due to the contribution from both electrostatic and Van der Waals energies with values of −3.74 and −1.17 kcal/mol, respectively, and also hydrophobic contribution to solvation free energy by the side chain of this residue with value of −1.34 kcal/mol. As mentioned earlier, both Ile553 and Hie252 are crucial amino acid residues which chelate with iron in the active site. Thus, distorting the geometry of these ligands could be the possible molecular mechanism for the inhibitory activity of tHGA. Additionally, Leu294, Leu248, Ile295 and Gln243, each contributed −2.42, −1.97, −1.81 and −1.72 kcal/mol, respectively, through the Van der Waals interactions from the side chains of the residues with the hydrophobic geranyl side chain of tHGA. The total non-polar solvation free energy of these residues are also interestingly high with values of −5.04 kcal/mol (Leu294), −4.02 kcal/mol (Leu248), −3.59 (Gln243) and −3.29 (Ile295), respectively. Results in the overall decomposition of free energy on a per-residue basis basically agreed well with the generated 2D diagram by LIGPLOT.[15] Therefore, the present study can be considered as a good model for understanding the way tHGA binds in the active site of the human 5-LOX enzyme (Fig. 9).

Table 2
Residue-based decomposition of the interaction energies (kcal/mol) for Van der Waals (ΔE_{vdw}), electrostatic (ΔE_{EEL}) and free binding energy ($\Delta G_{subtotal,GB}$) between tHGA and the residues in the binding pocket of 5-LOX model

Residue Number	ΔE_{vdw}	ΔE_{EEL}	$\Delta G_{subtotal,\ GB}$
GLN243	−1.72(0.27)	0.02 (0.16)	−3.59 (0.47)
THR244	−0.71 (0.15)	0.07 (0.05)	−1.31 (0.19)
HIE247	−0.84 (0.36)	0.14 (0.23)	−1.85 (0.25)
LEU248	−1.97 (0.32)	−0.90 (0.11)	−4.02 (0.45)
HIE252	−1.17 (0.66)	−3.74 (0.88)	−5.40 (0.69)
LEU253	−0.24 (0.12)	−0.17 (0.05)	−0.39 (0.23)
ILE286	−1.16 (0.19)	1.01 (0.16)	−1.90 (0.29)
ASN287	−1.06 (0.32)	0.50 (0.35)	−2.14 (0.33)
LYS289	−0.15 (0.02)	0.36 (0.27)	−0.43 (0.09)
ALA290	−0.99(0.29)	0.02 (0.12)	−2.15 (0.31)
LEU294	−2.42 (0.49)	−0.52 (0.15)	−5.04 (0.74)
ILE295	−1.81 (0.31)	−0.25 (0.09)	−3.29 (0.37)
GLY299	−0.08 (0.02)	−0.12 (0.03)	−0.18 (0.05)
LEU300	−0.62(0.14)	−0.06 (0.03)	−1.23 (0.23)
PHE301	−1.66 (0.42)	−0.37 (0.10)	−3.53 (0.42)
ASP302	−0.47 (0.15)	1.15 (0.25)	−0.62 (0.25)
ASN305	−0.49 (0.13)	−0.18 (0.07)	−1.07 (0.26)
HIE312	−0.92 (0.28)	0.05 (0.11)	−1.69 (0.34)
HIE430	−0.11 (0.01)	0.76 (0.08)	−0.19 (0.05)
ASN434	−0.25 (0.07)	−0.22 (0.64)	−0.72 (0.24)
GLN437	−0.10 (0.02)	−0.02 (0.06)	−0.17 (0.05)
ALA483	−0.30 (0.09)	−0.02 (0.05)	−0.71 (0.12)
ILE553	0.30 (0.79)	−13.45 (1.90)	−4.53 (1.38)

3. Conclusion

In conclusion, the bioassay-guided fractionation of the lipoxygenase enzyme inhibiting fraction of *M. ptelefolia* has resulted in the identification of tHGA as the bioactive compound. The compound significantly inhibited soybean 15-LOX and human 5-LOX and also shown to suppress the formation of CysLTs. tHGA showed only moderate DPPH activity and is not a metal-chelator, indicating a possible competitive (non-redox) mechanism for its interaction with 5-LOX. Non-redox type LOX inhibitors have been shown to have fewer side effects than redox or iron-chelating agents.[11] The observed inhibitory activity against both leukotriene and prostaglandin formation indicated that tHGA might act via a dual 5-LOX/COX mechanism, with a higher selectivity towards COX-2. Recently, Crockett et al.[16] also reported two structurally related acylphloroglucinols, which were also shown to be dual LOX/COX inhibitors with greater selectivity towards COX-1. However, despite a high degree of similarity in structures, tHGA demonstrated only moderate activity against COX-1 but maintained significant inhibitory activity against COX-2 and 5-LOX. These type of phloroglucinols, therefore, are favorable candidates for further drug development studies since dual inhibitors of both LOX and COX enzymatic pathways are expected to be more effective as anti-inflammatory agents and are expected to have better safety profile.[17,18] Recently, we have also demonstrated the effect of *M. ptelefolia* standardized extract against inflammatory pain in rats in vivo.[6] Results from the current study could explain in part this observed activity and in general, provides scientific evidence for the traditional usage of *M. ptelefolia* for treatment of inflammatory diseases.

4. Material and methods

4.1. General instrumentation and reagents

Aluminium sheets precoated with Silica Gel 60 F_{254} (20 × 20 cm, 0.2 mm thick; Merck) were used for TLC and silica gel PF_{254} (Merck) was used for vacuum liquid chromatography and preparative TLC. For enzyme inhibition assay, all chemicals used and lipoxygenase (1.13.11.12) type I-B (source: soybean) were purchased from Sigma (St. Louis, MO, USA). NMR and mass analysis was carried out using 500 MHz Varian Unity Inova and LCQ Finnigan Mat spectrometer, respectively.

4.2. Plant materials

The leaves of *M. ptelefolia* were collected from the medicinal plant garden of the Laboratory of Natural Products, Institute of Bioscience, Universiti Putra Malaysia. A voucher specimen (SK153/02) has been deposited at the herbarium of the Laboratory, authenticated by the Institute's botanist, Shamsul Khamis.

Air dried leaves (1.2 kg) of *M. ptelefolia* were pulverized and extracted by 48 h maceration with methanol at room temperature. The organic solvent was removed under reduced pressure, yielding

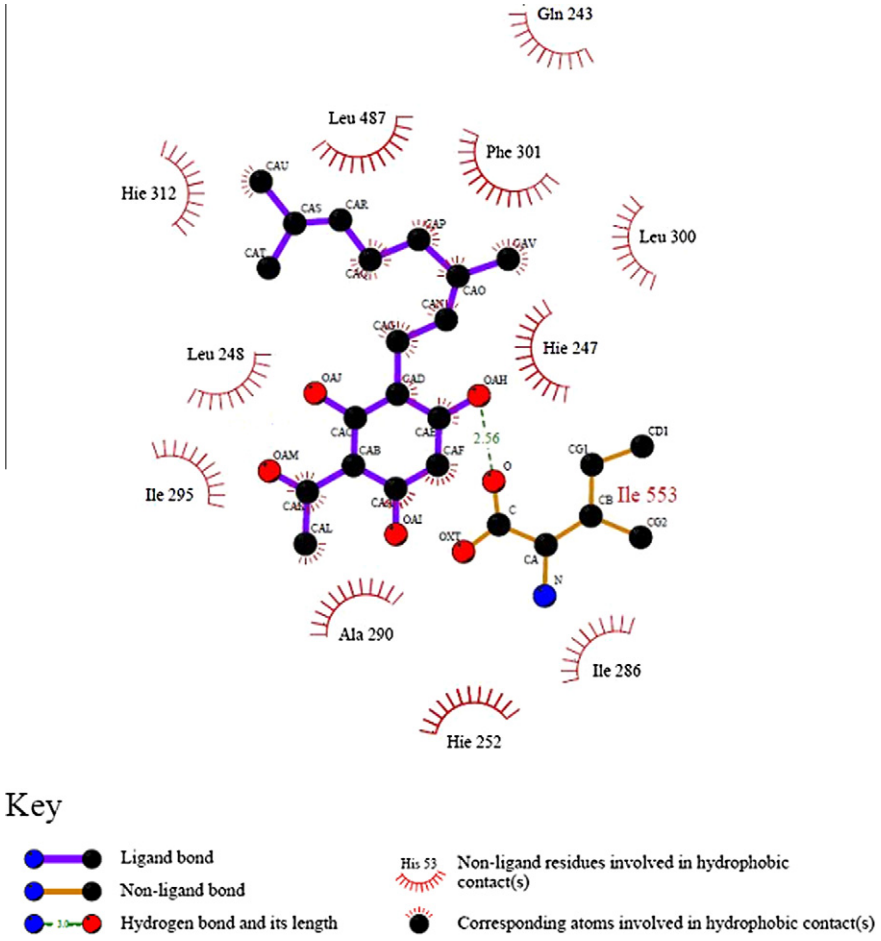

Figure 8. The 2D representation of the docking result of tHGA (**1**) with the residues in the active site of 5-LOX model shown by LIGPLOT.

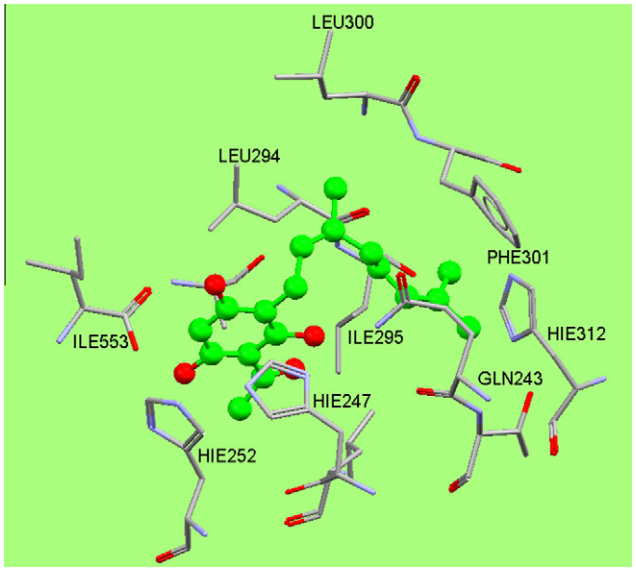

Figure 9. Ball and stick illustration of the interactions between tHGA (**1**) and the residues in the active site.

95.5 g of the crude methanolic extract (ca. 7.95% yield) which was then partitioned between water and *n*-hexane, CH_2Cl_2 and EtOAc. The solvent fractions were all assayed for soybean 15-LOX inhibition.

4.3. Bioassay-guided fractionation and isolation of compounds

The bioactive CH_2Cl_2 fraction was subjected to vacuum liquid chromatography using silica gel PF_{254}, eluted 100% hexane followed with stepwise gradient of CH_2Cl_2–EtOAc (100:0–0:100, v:v). The 70:30 eluate (2.5 g) tested positive against the 15-LOX assay and was purified further on Sephadex LH-20 (removal of chlorophyll) and preparative TLC (silica gel PF_{254}), to afford tHGA (**1**) (25.6 mg), *p*-*O*-geranylcoumaric acid (98 mg), kokusaginine (10 mg) and scoparone (8 mg). Only tHGA tested positive against 15-LOX. The identities of the compounds were confirmed by high resolution NMR and mass spectroscopy and comparison with literature data.[3] All of the isolated compounds were assayed against 15-LOX inhibition to determine their anti-inflammatory activity.

4.4. In vitro enzyme inhibition assays

The soybean enzyme (15-LOX) assay was performed in our lab while the human 5-LOX, COX-1 and COX-2 enzymes assays (Supplementary data Table 2) were performed by MDS Pharma Services (Taiwan, now Ricerca Biosciences). The protocols for the human enzyme assays, described herein, were provided by the company.

4.4.1. Soybean 15-LOX inhibition assay

In vitro 15-LOX inhibiting activity was measured using spectrophotometric method.[19] Sodium phosphate buffer (160 μL, 100 mM, pH 8.0), test sample (10 μL) and soybean lipoxygenase (1.13.11.12) type I-B solution (20 μL, 80 U/well) were mixed and incubated for 10 min at 25 °C. The reaction was then initiated by the addition of

the substrate in the form of linoleic acid (10 μL, 300 mM) solution. The enzymatic conversion of linoleic acid to form (9Z,11E)-(13*S*)-13-hydroperoxyoctadeca-9,11-dienoate was followed by the change of absorbance measured at 234 nm over a period of 6 min. Test samples and reference standards were dissolved in MeOH. Stock solutions were prepared at concentration 100 mg/mL for extract and 25 mg/mL for pure compounds. For solvent fractions, test concentrations were prepared from the stock by two-fold serial dilutions to give final concentrations of 100, 50, 25, 12.5, 6.3, 3.1, 1.6 μg/mL. Pure compounds were tested at a final concentration of 25 μg/mL and for compound showing bioactivity, the IC_{50} value was determined from tests concentrations of 25, 12.5, 6.25, 0.8, 0.4 μg/mL. All reactions were performed in triplicates in a 96-well microtitre plate. The IC_{50} was calculated from a plot of the sample concentration (μg/ml) versus percentage of inhibition (%) which is given by the formula:

$$\text{Inhibitory}\% = (\text{OD}_{\text{control}} - \text{OD}_{\text{sample}})/\text{OD}_{\text{control}}$$

4.4.2. Human 5-lipoxygenase (5-LOX) inhibition assay

Human peripheral blood mononuclear leukocytes (PBML) were used. tHGA (μM) and vehicle is preincubated with cells (5×10^6 cells/ml) in HBSS buffer for 15 min at 37 °C. The reaction was initiated by addition of 30 μM calimycin (A 23187) for another 15 min incubation period and was terminated by the addition of 1 N HCl. An aliquot was removed and the amount of LTB_4 formed was determined spectrophotometrically by an EIA kit. The method was adapted from Carter et al.[20] and Safayhi et al.[21]

4.4.3. Human cyclooxygenase-1 (COX-1) inhibition assay

Human platelets were used. Test compound and/or vehicle were incubated with cells (5×10^7/ml) in HBSS buffer (15 mM, pH 7.4) for 15 min at 37 °C. The reaction is initiated by the addition of 100 μM arachidonic acid for another 15 min incubation period and terminated by further addition of 1 N HCl. An aliquot was removed and the amount of PGE_2 formed determined spectrophotometrically by EIA kit. Compounds were screened at 10 μM. The method was adapted from Chan[22] and Swinney et al.[23]

4.4.4. Human cyclooxygenase-2 (COX-2) inhibition assay

Human recombinant cyclooxygenase expressed in Sf21 cells (Sigma, C-0858) was used. Test compound and/or vehicle was preincubated with 0.11U cyclooxygenxe-2, 1 mM reduced GSH, 500 μM phenol and 1 μM hematine for 15 min at 37 °C in Tris–HCl (100 mM, pH 7.7). The reaction was initiated by the addition of 0.3 mM arachidonic acid and terminated after 5 min by further addition of 1 N HCl. Following centrifugation, substrate conversion to PGE_2 is measured using an Amersham EIA kit. Compounds were screened at 10 μM. The method was adapted from Riendeau et al.[24] and Warner et al.[25]

4.5. In vitro inhibition of cysteinyl leukotriene (CysLTs) produc tion assay

4.5.1. Preparation of mouse macrophages

Inhibition of CysLTs production was measured according to Benito et al.[26] NMRI male mice (20 ± 5 g) were injected intraperitoneally (ip) with 1 ml of thioglycolate broth, and kept for 3 days for stimulation. After 3 days, all mice were killed by cervical dislocation and their macrophages were collected by peritoneal lavage with phosphate buffer saline (PBS). PBS was injected into the peritoneum and the cavity was gently massaged for 1 min. The lavage fluid was aspirated and the cells were isolated by centrifugation (1000 rpm, 4 °C, 10 min). The supernatant was decanted and the cells were counted and resuspended at 10^6 cells/ml in Dulbecco's modified Eagle's medium (DMEM) supplemented with 10% heat-inactivated fetal calf serum (FCS) (Sigma, USA). 50 μl of the cell suspension was transferred into a 96-well plate and incubated for 24 h at 37 °C in an atmosphere of 5% CO_2 to allow the cells to adhere to the plates.

4.5.2. CysLTs release and cell viability assays

5-LOX product formation was studied in calcium ionophore-stimulated mouse peritoneal macrophages, for the determination of cysLTs (LTC_4/LTD_4/LTE_4) synthesis. Macrophages at a cell density of 5×10^5 cells/well were prepared in a 96-well microtitre plate and left overnight for attachment. Non-adherent cells were removed by washing the cells with PBS and fresh DMEM (without FCS) was added. The cells were pre-incubated with each test compound for 60 min at 37 °C. Then, calcium ionophore A23187 (Sigma, USA) was added to reach a final concentration of 10^{-6} M and the cells were further incubated for 2 h. The medium from each well was collected directly from the plates, and centrifuged at 3000 rpm and 4 °C for 10 min. CysLTs in the supernatant of each reaction mixture were quantitated by an ELISA kit (Cayman Chemical Co., USA). Nordihydroguaiaretic acid (NDGA) was used as reference compound.

The viability of cells remaining in the wells was assessed by using 3-(4,5-dimethyl-thiazol-2-yl)-2,5-diphenyltetrazolium bromide (MTT)-based colorimetric assay. Twenty microliter of MTT solution (5 mg/ml in phosphate buffered saline) was added into each well and further incubated for 4 h at 37 °C. After aspirating the supernatant from the wells, 100 μl of DMSO were added for the dissolution of formazan crystals. The absorbance of each well was then read at 550 nm using a microplate reader (VersaMax, Molecular Devices, Sunnyvale, California, USA). LTC_4 concentrations were assessed directly from a standard curve. Data are shown as mean ± S.D. of groups in most cases triplicate determinations. Statistical analysis was performed using Student's *t*-test for unpaired data.

4.6. Free radical scavenging activity using DPPH assay

The DPPH assay was carried out according to previously described method.[27] Quercetin was used as positive control. Tests were performed in triplicates and the absorbances were averaged before calculation.

4.7. Metal chelating activity

Metal-chelating property was measured according to the method described by Brown et al.[28] with some modifications. The property was recorded for $FeSO_4$, $CuSO_4$ and $FeCl_3$ solutions. A stock solution of the test compound was prepared in methanol (1 mM). Then, 50 μM solutions were prepared in cuvettes with PBS (10 mM, pH 7.4). Absorption spectra were recorded from 200 to 600 nm after 10 s, with 50 and 100 μM of the salt solution. The results were compared with the spectrum of the test compound alone.

4.8. Ligand–enzyme interaction studies

4.8.1. Construction and refinement of the structure model

The construction of the homology modeling was started with the searching of human LOX-5 amino acids sequence. The amino acids sequence of human 5-LOX (Accession Id: P009917) was retrieved from UniProtKB.[29] Then, BLAST program was used to search for the suitable template structure in the Protein Data Bank (PDB) at National Center for Biotechnology Information, NCBI (www.ncbi.nih.gov) for the homology modeling of human 5-LOX. Delta413417GS I805W LOX (pdb id: 3fg3A)[30] resulted in 40% same

identities and 60% positives with human 5-LOX and therefore it was chosen as the template. Alignment of the amino acids sequence into the template crystal structure of 3fg3A was performed using the align2d function in EasyModeller 2.0 where ten 3D models of 5-LOX were generated.[31] This improved dynamic programming algorithm was based on a variable gap penalty function that tends to place gaps in solvent exposed and curved regions which decrease the alignment error in standard alignment method. Generated models were further improved through the loop modeling followed by model optimization using the modified version of the Beale restart conjugate gradients method. The model profile plots were generated and analyzed. The lowest DOPE energy of the loaded models was then taken into docking and MD simulation.

4.8.2. Molecular docking

The ligand tHGA (1) was constructed and energy minimized using MOPAC program with MMFF94 force field calculation. The ligand was docked into the active site of the homology model using GOLD4.1.[32] The binding site was defined based on the cavity detection by GOLD centered on the active site and the atoms selection was restricted to solvent-accessible surface. All other parameters were set up according to the standard protocols of GOLD. The standard docking procedure includes the use of genetic algorithm to explore the full range of ligand conformational flexibility with the partial flexibility of protein while the scoring function includes the terms for hydrogen-bonding, Van der Waals, and intramolecular energies. Ten top ranked poses results were saved and evaluated. The highest GOLD fitness score was chosen as a resultant coordinate and equilibrated.

4.8.3. Molecular simulation

The starting structure was the docked structure of tHGA (1) and 5-LOX obtained from GOLD. The parameterization of tHGA (1) was carried out using R.E.D. III[33] and Antechamber[34] module implemented in AMBER 8.0 suite of programs.[35] The xLEaP[36] module in AMBER 8.0 was used to prepare the input files for MD simulations. The Wang et al.[37] force field (also known as *ff09*) represented the molecular mechanical potentials. The prepared complex structure was then immersed in a 10 Å isomeric truncated octahedral box of pre-equilibrated TIP3P water.[38] The initial solvated structure was subjected to 2000 steps energy minimization with position restraints (500 kcal/mol) on the protein followed by 5000 steps minimization with restraints on residues 247, 252, 430, and 535 using steepest-descent and conjugate-gradient techniques.

Molecular dynamics simulations were performed at 300 K by using SANDER module in the program AMBER 8.0. The minimized structures were subjected to an equilibration protocol in which the temperature of the system was gradually increased from 0 K to 300 K for 20 ps while holding both the volume and temperature constant, followed by a solvent density adjustment for 50 ps at 300 K by holding the temperature and pressure constant while allowing the volume to change. Langevin thermostat was used to maintain the temperature and pressure.[39] The production simulations of 3.4 ns at 1 fs timestep were then performed in an isothermal-isobaric (NPT) ensemble using periodic boundary conditions to reduce edge effect and simulate a semi-dilute solvent environment based on the Particle Mesh Ewald (PME) method for treating the long range electrostatic interactions.[40] SHAKE algorithm[41] was used to constrain the bonds involving hydrogen atoms.

The MD trajectories was analyzed by calculating the evolution of structural properties over time including the backbone atoms root mean square deviations (Cα-RMSd) and the root mean square fluctuations (RMSf) using Ptraj module in the program AMBER 8.0.

4.8.4. MM-PBSA calculations

A single trajectory approach was adopted in the calculation of the binding free energies between the receptor and inhibitors according to the snapshots taken during the performed MD trajectory. In the MM-PBSA method,[42,43] the binding free energy (ΔG_{bind}) (2) could be approximated by summing the average energy of molecular mechanics (ΔE_{MM}), the solvation free energy (ΔG_{solv}), and the vibrational entropy term ($T\Delta S$). ΔE_{MM} (3) represented the average molecular mechanics energy contributed by bonded (E_{bond},E_{angle}, and $E_{torsion}$) and non-bonded (E_{vdw}, and E_{EEL}). ΔG_{solv}(4) is represented by summing of polar solvation free energy evaluated using the Poisson–Boltzmann equation, ΔG_{PB}, and non-polar contribution to solvation free energy from the surface area, ΔG_{SA}(5). *pbsa* program in AMBER 8.0 was used to calculate the polar contribution (ΔG_{PB}). The dielectric constant was set to 1 for interior solute and 80 for exterior water. MSMS algorithm was used to estimate the solvent-accessible surface area (SASA) with probe radius of 1.4 Å.The surface tension proportionality constant γ was set to 0.0072 kcal/mol/Å^2 to calculate total nonpolar solvation energy. Decomposition of interaction energies between tHGA and adjacent residues was done using MM-GBSA calculation, where the ΔG_{PB} is replaced with ΔG_{GB}. The overall equations could be summarized as follows:

$$\Delta G_{bind} = G_{com} - G_{rec} - G_{lig} \quad (1)$$

$$\Delta G = \Delta E_{MM} + \Delta G_{Solv} - T\Delta S \quad (2)$$

In which:

$$\Delta E_{MM} = \Delta E_{bond} + \Delta E_{angle} + \Delta E_{torsion} + \Delta E_{vdw} + \Delta E_{EEL} \quad (3)$$

$$\Delta G_{solv} = \Delta G_{PB} + \Delta G_{SA} \quad (4)$$

$$\Delta G_{SA} = \gamma SA + b \quad (5)$$

Acknowledgments

The authors thank the Malaysian Ministry of Science, Technology, and Environment (MOSTI) for providing research grant under IPHARM R&D Initiatives.

Supplementary data

Supplementary data associated with this article can be found, in the online version, at doi:10.1016/j.bmc.2011.09.001.

References and notes

1. (a) Whitmore, T. C. In *A Manual for Forester*; Longman Press, 1972; Vol. 1,; (b) Loi, D T. *Nhung chay thoue va vi thoue Vietnam (Glossary of Vietnamese medicinal plants)*; Science and Technics Publication: Hanoi, 1977; (c) Perry, L. M.; Metzger, J. *Medicinal Plants of East and Southeast Asia: Attributed Properties and Uses*; MIT Press: Cambridge, 1980.
2. Irmawati, R.; Kamarulzaman, N. H.; Khozirah, S.; Ee, G. C. L. *Nat. Prod. Res.* **2004**, *18*, 289.
3. Khozirah, S.; Suryati, S.; Faridah, A.; Lajis, N. H.; Israf, D. A. *Nat. Prod. Res.* **2006**, *20*, 415.
4. (a) Faridah, A.; Lajis, N. H.; Israf, D. A.; Khozirah, S.; Umi Kalsom, Y. *Food Chem.* **2006**, *95*, 566; (b) Faridah, A.; Khozirah, S.; Israf, D. A.; Suryati, S.; Zurina, Z.; Lajis, N. H. *J. Food Composition Anal.* **2010**, *23*, 107.
5. (a) Manandhar, M. D.; Hussaini, F. A.; Kapil, R. S.; Shoeb, A. *Phytochemistry* **1985**, *24*, 199; (b) Kumar, V.; Karunaratne, V.; Sanath, M. R.; Meegalle, M.; Macleod, J. K. *Phytochemistry* **1990**, *29*, 243.
6. Mohd Roslan, S.; Azyyati, M. P.; Khozirah, S.; Syamimi, K.; Wan Mastura, S. M.; Azam Shah, M.; Syahida, A.; Ahmad, A.; Daud, I.; Lajis, N. H. *J. Biomed. Biotechnol.* **2010**, doi:10.1155/2010/937642.
7. (a) Samuelson, B.; Dahlen, S.-E.; Lidgren, J. A.; Rouzer, C. A.; Serhan, C. N. *Science* **1987**, *237*, 1171; (b) Schneider, C.; Pratt, D. A.; Porter, N. A.; Brash, A. R. *Chem. Biol.* **2007**, *14*, 473.
8. Kanaoka, Y.; Boyce, A. J. *J. Immunol.* **2004**, *173*, 1503.
9. (a) Jampilek, J.; Dolezal, M.; Opletalova, V.; Hartl, J. *Curr. Med. Chem.* **2006**, *13*, 117; (b) Lewis, R. A.; Austen, K. F.; Soberman, R. J. *N. Eng. J. Med.* **1990**, *323*, 645; (c) Welsch, D. J. *Proc. Natl. Acad. Sci.* **1994**, *91*, 9745.
10. (a) Guidelines for the diagnosis and management of asthma. National Heart, Lung and Blood Institute. Expert panel Report, National Asthma Education Program. *J. Allergy Clin. Immunol.* **1991**, *88*, 425.; (b) Calanni, F.; Laufer, S. Inflammation and Rheumatic Diseases. In *The Molecular Basis of Novel*

In Laufer, S., Gay, S., Brune, K., Eds.; Georg Thieme: Stuttgart, Germany, 2003; pp 15–57; (c) Werz, O. *Planta Med.* **2007**, *73*, 1331.
11. McMillan, R. M.; Walker, E. R. H. *Trends Pharmacol. Sci.* **1992**, *13*, 323.
12. Vane, J. R.; Botting, R. M. *Scand. J. Rheumatol.* **1996**, 9.
13. Charles, B.; Sundel, R. Technical Corner from IASP Newsletter. Sept/Oct. 1998 (www.iasp-pain.org//AM/Template.cfm?Section=Home).
14. Zhang, Y. Y.; Lind, B.; Radmark, O.; Samuelsson, B. *J. Biol. Chem.* **1993**, *268*, 2535.
15. Wallace, A. C.; Laskowski, R. A.; Thornton, J. M. *Protein Eng.* **1995**, *8*, 127.
16. Crockett, S.; Wenzig, E.-M.; Kunert, O.; Bauer, R. *Phytochem. Lett.* **2008**, *1*, 37.
17. Chalrier, C.; Michaux, C. *Eur. J. Med. Chem.* **2003**, *38*, 645.
18. Dyer, R. D.; Connor, D. T. *Curr. Pharm. Des.* **1997**, *3*, 463.
19. Riaz, N.; Malik, A.; Rehman, A. U.; Ahmed, Z.; Muhammad, P.; Nawaz, S. A.; Siddique, J.; Choudhary, M. I. *Phytochemistry* **2004**, *65*, 1129.
20. Carter, G. W.; Young, P. R.; Albert, D. H.; Bouska, J.; Dyer, R.; Bell, R. L.; Summers, J. B.; Brooks, D. W. *J. Pharmacol. Exp. Ther.* **1991**, *256*, 929.
21. Safayhi, H.; Boden, S. E.; Schweizer, S.; Ammon, H. P. T. *Planta Med.* **2000**, *66*, 110.
22. Chan, C.-C. *J. Pharmacol. Exp. Ther.* **1999**, *290*, 551.
23. Swinney, D. C.; Mak, Y.; Barnett, J.; Ramesha, C. S. *J. Biol. Chem.* **1997**, *272*, 12393.
24. Riendeau, D.; Charleson, S.; Cromllsh, W.; Mancini, J. A.; Wong, E.; Guay, J. *Can. J. Physiol. Pharmacol.* **1997**, *75*, 1088.
25. Warner, T. D.; Giuliano, F.; Vojnovic, I.; Bukasa, A.; Mitchell, J. A.; Vane, J. R. *Proc. Natl. Acad. Sci. U.S.A.* **1999**, *96*, 7563.
26. Benito, P. B.; Abad, M. J.; Diaz, A. M.; Villaescusa, L.; Gonzales, M. A.; Silvan, A. M. *Biol. Pharm. Bull.* **2002**, *25*, 1.
27. Cottelle, N.; Bernier, J. L.; Catteau, J. P.; Pommery, P.; Wallet, J. C.; Gaydou, E. M. *Free Radical Biol. Med.* **1996**, *20*, 35.
28. Brown, J. E.; Khodr, H.; Hider, R. C.; Rice-Evans, C. A. *Biochem. J.* **1998**, *330*, 1173.
29. The Universal Protein Resource (UniProt). *Nucleic Acids Res.* **2009**, *37*, D169.
30. Neau, D. B.; Gilbert, N. C.; Bartlett, S. G.; Boeglin, W.; Brash, A. R.; Newcomer, M. E. *Biochemistry* **2009**, *48*, 7906.
31. Sali, A.; Blundell, T. L. *J. Mol. Biol.* **1993**, *234*, 779.
32. Verdonk, M. L.; Cole, J. C.; Hartshorn, M. J.; Murray, C. W.; Taylor, R. D. *Proteins* **2003**, *52*, 609.
33. Dupradeau, F. Y.; Pigache, A.; Zaffran, T.; Savineau, C.; Lelong, R.; Grivel, N.; Lelong, D.; Rosanski, W.; Cieplak, P. *Phys. Chem. Chem. Phys* **2010**, *12*, 7821.
34. Wang, J.; Wang, W.; Kollman, P. A.; Case, D. A. *J. Mol. Graphics Modell.* **2006**, *25*, 247.
35. Case, D. A.; Cheatham, T. E., 3rd; Darden, T.; Gohlke, H.; Luo, R.; Merz, K. M., Jr.; Onufriev, A.; Simmerling, C.; Wang, B.; Woods, R. J. *J. Comput. Chem.* **2005**, *26*, 1668.
36. Schafmeister, C.E.A.F.R., W.S.; Romanovski, V. *University of California at San Fransisco, USA.* **1995**.
37. Wang, J.; Cieplak, P.; Kollman, P. A. *J. Comput. Chem.* **2000**, *21*, 1049.
38. Jorgensen, W. L. C. J.; Madura, J.; Klein, M. L. *J. Chem. Phys.* **1983**, *79*, 926.
39. Pastor, R. W. B. B. R.; Szabo, A. *Mol. Phys.* **1988**, *65*, 1409.
40. Essmann, U. P. L.; Berkowitz, M. L.; Darden, T.; Lee, H.; Pedersen, L. G. *J. Chem. Phys.* **1995**, *103*, 8577.
41. Ryckaert, J. P. C.; Berendsen, H. J. C. *J. Comput. Phys.* **1977**, *23*, 327.
42. Kollman, P. A.; Massova, I.; Reyes, C.; Kuhn, B.; Huo, S.; Chong, L.; Lee, M.; Lee, T.; Duan, Y.; Wang, W.; Donini, O.; Cieplak, P.; Srinivasan, J.; Case, D. A.; Cheatham, T. E., 3rd *Acc. Chem. Res.* **2000**, *33*, 889.
43. Wang, J.; Morin, P.; Wang, W.; Kollman, P. A. *J. Am. Chem. Soc.* **2001**, *123*, 5221.